Biophysical Journal, Volume 99

Supporting Material

Uncovering specific electrostatic interactions in the denatured states of proteins

Jana K Shen

Uncovering specific electrostatic interactions in the denatured states of proteins

Jana K. Shen [1]
Department of Chemistry and Biochemistry
University of Oklahoma
Norman, OK 73019, USA

Simulation protocols

All simulations were performed using the continuous constant pH molecular dynamics (CPHMD) method (1–3) as implemented in the CHARMM molecular dynamics program (4). Temperature replica-exchange (REX) enhanced sampling protocol (5) was enabled through a Perl interface as implemented in the MMTSB toolset (1, 6). The CHARMM22/CMAP protein force field (7, 8) was used for energy and force evaluations. Solvent effects were modeled by the GBSW implicit-solvent model with the default parameters (9, 10). The hydrophobic contribution to solvation free energy was calculated using the surface area model with a surface tension coefficient of 0.005 kcal/mol·Å^2 consistent with previous GBSW simulations of proteins (10–12). Dynamics was propagated with a time step of 2 fs using the Langevin algorithm with a friction coefficient of 5 ps^{-1} for all heavy atoms consistent with previous GBSW folding simulations (10–12). Nonbonded interactins were smoothly switched off over the range of 22-24 Å using a switching function.

Simulations of native and denatured states of WT and K12M NTL9

REX-CPHMD simulations for the denatured states of WT and K12M NTL9 were carried out at pH 4 and 100 mM salt concentration starting from 20 replicas in the extended conformations with different initial velocity seeds. The REX protocol utilized the exponentially-spaced temperature range of 298–450 K and the frequency of exchange attempts was 2 ps. The average exchange ratio was about 50%. Sampling of each replica lasted 65 ns resulting in an aggregated simulation time of 1.3 μs. Spatial and titration coordinates were collected every 2 ps from the 298 K window. Unless otherwise noted, data from the first 15 ns was discarded in the analysis.

Titration simulations for the native states of WT and K12M NTL9 were performed at pH 2, 3 and 4 starting from the crystal structures for WT (residues 1–52, PDB ID: 2HBB) and K12M mutant (PDB ID: 2HBA, sequence 1–52) as well as the NMR model for WT (residues 1–56, PDB ID: 1CQU) and the corresponding computationally mutated model for the mutant. The same REX protocol as for the denatured states was used. The simulation time was 2 ns per replica. Data from the first 500 ps was discarded in the pK_a calculations.

Simulations of fragment peptides

REX-CPHMD simulations for the fragment peptides were carried out at pH 4 and 100 mM salt concentration starting from 8 replicas in the extended conformations. The sequences and blocking groups were identical to those used in the experimental work (13): NH_3-^{1}MKVIFLKDVKG^{11}-NH_2,

[1]Phone: (405) 325-0458; E-mail: jana.k.shen@ou.edu

Ac-^{12}GKGKKGEIKNVAD^{23}-NH_2, Ac-^{21}VADGYAN^{27}-NH_2, Ac-^{35}LAIEATPA^{42}-NH_2,
and Ac-^{40}TPANLKALEAQKQKEQR^{56}-NH_2. The same temperature range and exchange frequency were used as for the intact proteins. The simulation length for each replica was 40 ns, resulting in an aggregated time of 320 ns. Data from the last 20 ns simulation was used for pK_a calculations.

Sequences 1-11 and 12-23 encompass the N-terminal β-sheet and loop region in NTL9, while sequences 21-27 and 40-56 form helical segments. Sequence 35–42 forms a β-strand in NTL9. Based on our previous experience with GBSW folding simulations of peptides (10–12), and by monitoring the time series of helical content and pK_a's, the total simulation time for the fragments is long enough to ensure sampling convergence. We compare the calculated total helical content to experiment (Table S1). Fragments 21-27 and 35-42 show negligible helicity in simulations, in agreement with NMR and CD data (13). The simulation of fragment 40-56 gives a total helicity of 55%, slightly higher than the estimated percentage (40%) based on the CD data (13). The simulations of fragments 1-11 and 12-23 overestimate the total helical content in comparison to the CD and NMR data (13), which can be attributed to the helical bias problem due to the employed CHARMM force field and GBSW solvent model. Next, we compare the calculated pK_a's of the fragments with those from NMR titrations (Table S1). As expected, the pK_a's of acidic groups are all underestimated. The largest deviation is -0.60 pH units for Glu48. Given the estimated statistical uncertainty of 0.16 pH units for REX-CPHMD simulations (1), the discrepancies indicate a systematic overstabilization of attractive electrostatic interactions that are local in sequence. We reasoned that, since the denatured state is largely devoid of tertiary interactions, errors manifested at the local level are likely dominant in the simulation of the denatured state of the intact protein. Consequently, we used the deviations found for fragment peptides to calibrate the calculations of denatured-state pK_a's of WT and K12M NTL9.

Table S1: Summary of pK_a values for the fragment peptides of NTL9

Residue	Fragment	pK_a			Helical content	
		Calc	Expt	Dev	Calc	Expt
Asp8	1–11	3.79	3.84	-0.05	0.50	neg.
Glu17	12–23	3.75	4.11	-0.36	0.33	neg.
Asp23	21-27	3.91	4.11	-0.20	0.06	neg.
Glu38	35–42	4.29	4.63	-0.34	0.09	neg.
Glu48	40–56	3.71	4.31	-0.60	0.55	0.40
Glu54	40–56	3.93	4.32	-0.39	0.55	0.40

Experimental values are taken from Ref (13, 14). Helicity calculation was based on the DSSP assignment (15).

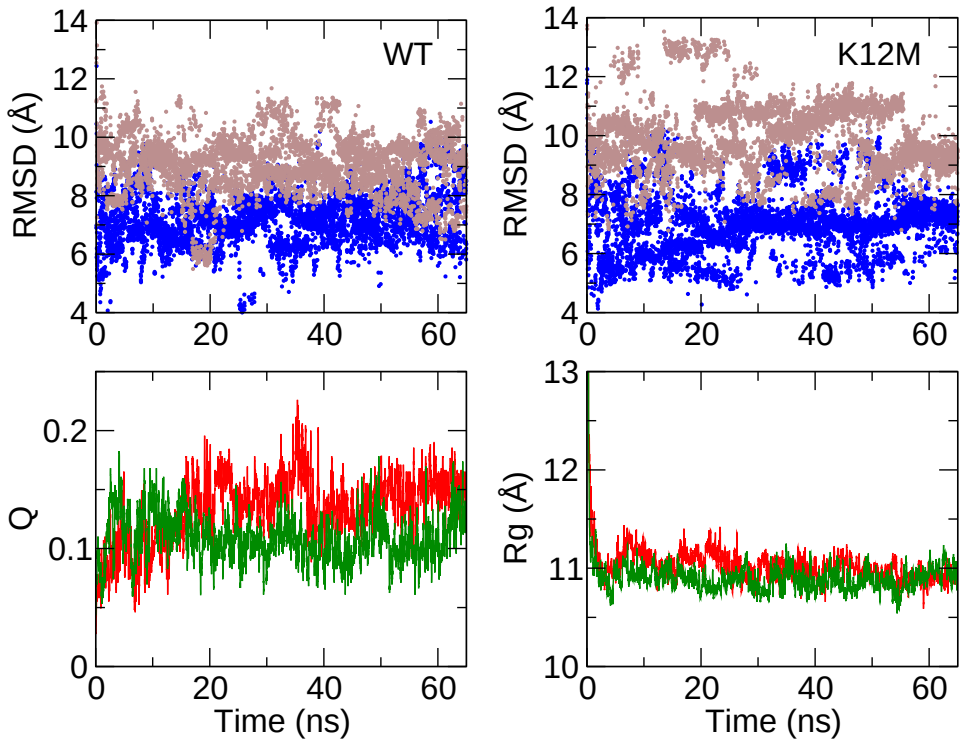

Figure S1: Time series of order parameters. Top. Cα RMSD of segment A (blue) and B (brown) in WT and K12M NTL9 with respect to the native structures as a function of simulation time. Bottom. Fraction of native contacts (Q) as well as radius of gyration (R_g) as a function of simulation time for WT (red) and K12M (green) NTL9. A pair of non-adjacent residues are defined as in contact if the minimum distance between side-chain atoms (or Cα atom for Gly) is closer than 4.5 Å.

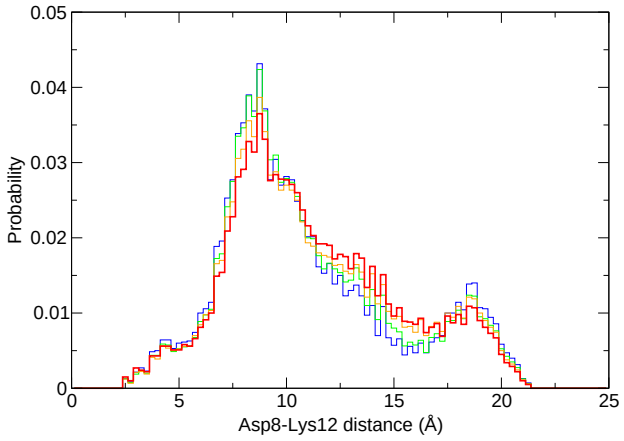

Figure S2: Convergence of the probability distribution for the distance between Asp8 and Lys12 in WT NTL9. Histograms were constructed using the data from 15-50 ns (blue), 15-55 (green), 15-60 (orange), and 15-65 ns (red). The distance was calculated between either of the carboxylate oxygens in Asp8 and the amino nitrogen in Lys12.

Table S2: Convergence of calculated denatured-state pK_a values for WT NTL9

Time	Asp8	Glu17	Asp23	Glu38	Glu48	Glu54
50	3.10	3.95	4.02	3.79	4.41	4.12
55	3.18	3.91	4.02	3.82	4.44	4.14
60	3.18	3.91	3.99	3.84	4.46	4.14
65	3.22	3.93	3.95	3.86	4.50	4.16

Time refers to the total sampling time per replica in ns with the first 15 ns discarded. The random error is estimated to be 0.16 pK_a units (1).

Table S3: Convergence of calculated denatured-state pK_a values for K12M NTL9

Time	Asp8	Glu17	Asp23	Glu38	Glu48	Glu54
50	3.91	4.05	3.83	3.95	4.89	4.25
55	3.91	4.05	3.83	4.01	4.83	4.25
60	3.86	4.09	3.87	4.05	4.78	4.25
65	3.80	4.11	3.91	4.11	4.74	4.25

Time refers to the total sampling time per replica in ns with the first 15 ns discarded. The random error is estimated to be 0.16 pK_a units (1).

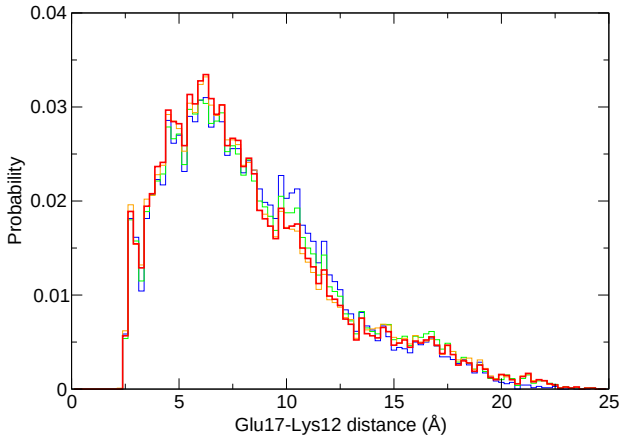

Figure S3: Convergence of the probability distribution for the distance between Glu17 and Lys12 in WT NTL9. Histograms were constructed using the data from 15-50 ns (blue), 15-55 (green), 15-60 (orange), and 15-65 ns (red). The distance was calculated between either of the carboxylate oxygens in Glu17 and the amino nitrogen in Lys12.

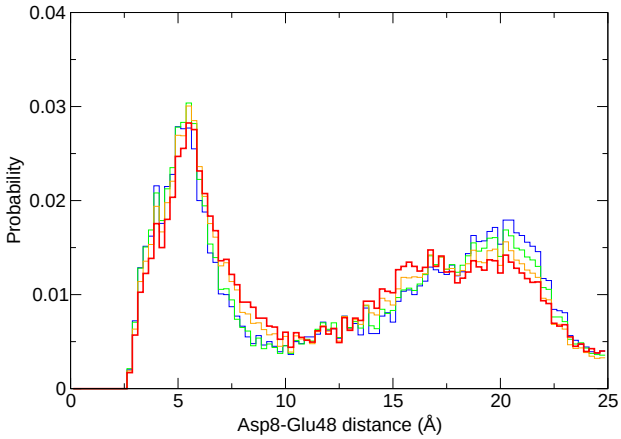

Figure S4: Convergence of the probability distribution for the distance between Asp8 and Glu48 in K12M NTL9. Histograms were constructed using the data from 15-50 ns (blue), 15-55 (green), 15-60 (orange), and 15-65 ns (red). The distance was calculated between either of the carboxylate oxygens in Asp8 and Glu48.

References

1. Khandogin, J., and C. L. Brooks III, 2006. Toward the accurate first-principles prediction of ionization equilibria in proteins. *Biochemistry* 45:9363–9373.

2. Lee, M. S., F. R. Salsbury, Jr., and C. L. Brooks III, 2004. Constant-pH molecular dynamics using continuous titration coordinates. *Proteins* 56:738–752.

3. Khandogin, J., and C. L. Brooks III, 2005. Constant pH molecular dynamics with proton tautomerism. *Biophys. J.* 89:141–157.

4. Brooks, B. R., C. L. Brooks III, A. D. Mackerell, Jr., L. Nilsson, R. J. Petrella, B. Roux, Y. Won, G. Archontis, C. Bartles, S. Boresch, A. Caflisch, L. Caves, Q. Cui, A. R. Dinner, M. Feig, S. Fischer, J. Gao, M. Hodoscek, W. Im, K. K. T. Lazaridis, J. Ma, V. Ovchinnikov, E. Paci, R. W. Pastor, C. B. Post, J. Z. Pu, M. Schaefer, B. Tidor, R. M. Venable, H. L. Woodcock, X. Wu, W. Yang, D. M. York, and M. Karplus, 2009. CHARMM: The biomolecular simulation program. *J. Comput. Chem.* 30:1545–1614.

5. Sugita, Y., A. Kitao, and Y. Okamoto, 2000. Multidimensional replica-exchange method for free-energy calculations. *J. Chem. Phys.* 113:6042–6051.

6. Feig, M., J. Karanicolas, and C. L. Brooks, III, 2004. MMTSB tool set: enhanced sampling and multiscale modeling methods for applications in structure biology. *J. Mol. Graph. Model.* 22:377–395.

7. MacKerell, Jr., A. D., D. Bashford, M. Bellott, R. L. Dunbrack, Jr., J. D. Evanseck, M. J. Field, S. Fischer, J. Gao, H. Guo, S. Ha, D. Joseph-McCarthy, L. Kuchnir, K. Kuczera, F. T. K. Lau, C. Mattos, S. Michnick, T. Ngo, D. T. Nguyen, B. Prodhom, W. E. Reiher, III, B. Roux, M. Schlenkrich, J. C. Smith, R. Stote, J. Straub, M. Watanabe, J. Wiórkiewicz-Kuczera, D. Yin, and M. Karplus, 1998. All-atom empirical potential for molecular modeling and dynamics studies of proteins. *J. Phys. Chem. B* 102:3586–3616.

8. Mackerell, Jr., A. D., M. Feig, and C. L. Brooks, III, 2004. Extending the treatment of backbone energetics in protein force fields: Limitations of gas-phase quantum mechanics in reproducing protein conformational distributions in molecular dynamics simulations. *J. Comput. Chem.* 25:1400–1415.

9. Im, W., M. S. Lee, and C. L. Brooks III, 2003. Generalized Born model with a simple smoothing function. *J. Comput. Chem.* 24:1691–1702.

10. Chen, J., W. Im, and C. L. Brooks III, 2006. Balancing solvation and intramolecular interactions: toward a consistent generalized Born force field. *J. Am. Chem. Soc.* 128:3728–3736.

11. Khandogin, J., J. Chen, and C. L. Brooks III, 2006. Exploring atomistic details of pH-dependent peptide folding. *Proc. Natl. Acad. Sci. USA* 103:18546–18550.

12. Khandogin, J., and C. L. Brooks III, 2007. Linking folding with aggregation in Alzheimer's beta amyloid peptides. *Proc. Natl. Acad. Sci. USA* 104:16880–16885.

13. Kuhlman, B., D. L. Luisi, P. Young, and D. P. Raleigh, 1999. pK_a values and the pH dependent stability of the N-terminal domain of L9 as probes of electrostatic interactions in the denatured state. Differentiation between local and nonlocal interactions. *Biochemistry* 38:4896–4903.

14. Cho, J.-H., S. Sato, and D. P. Raleigh, 2004. Thermodynamics and kinetics of non-native interactions in protein folding: a single point mutant significantly stabilizes the N-terminal domain of L9 by modulating non-native interactions in the denatured state. *J. Mol. Biol.* 338:827–837.

15. Kabsch, W., and C. Sander, 1983. Dictionary of protein secondary structure: Pattern recognition of hydrogen-bonded and geometrical features. *Biopolymers* 22:2577–2637.